Applied Catalysis B: Environmental 257 (2019) 117888

Contents lists available at ScienceDirect

Applied Catalysis B: Environmental

journal homepage: www.elsevier.com/locate/apcatb

Synergistic effect of metal-organic framework-derived boron and nitrogen heteroatom-doped three-dimensional porous carbons for precious-metal-free catalytic reduction of nitroarenes

Chi Van Nguyen[a], Seulchan Lee[b], Yongchul G. Chung[b,**], Wei-Hung Chiang[a,**], Kevin C.-W. Wu[c,d,e,*]

[a] Department of Chemical Engineering, National Taiwan University of Science and Technology, No. 43, Sec. 4, Keelung Road, Taipei, 10607, Taiwan
[b] School of Chemical and Biomolecular Engineering, Pusan National University, 46241, Busan, South Korea
[c] Department of Chemical Engineering, National Taiwan University, No. 1, Sec. 4, Roosevelt Road, Taipei, 10607, Taiwan
[d] Center of Atomic Initiative for New Materials (AI-MAT), National Taiwan University, Taiwan
[e] International Graduate Program of Molecular Science and Technology, National Taiwan University (NTU-MST), Taiwan

ARTICLE INFO

Keywords:
Metal-organic framework (MOF)
Boron and nitrogen co-doped
Porous carbons
Metal-free catalyst
Catalytic 4-NP reduction

ABSTRACT

We report a scalable and controllable synthesis of metal-organic framework (MOF)-derived three-dimensional boron and nitrogen heteroatom-doped porous carbons (3D-BNPCs) and their synergistic effect for metal-free catalytic 4-nitrophenol (4-NP) reduction. The substitution of boron atoms into zeolitic imidazole framework-8 (ZIF-8)-derived nitrogen-doped porous carbon (B-NPC-1200) significantly improves the electrical conductivity and the catalytic 4-NP reduction. We propose the heteroatom-doping of boron, nitrogen and oxygen in the 3D- B-N PC catalysts creates synergistic effect on 4-NP reduction by creating more catalytically active sites. High-Resolution X-ray Photoelectron Spectroscopy (HR-XPS) and Density Functional Theory (DFT) calculations were carried out to confirm and investigate the role of active sites on adsorption of 4-NP molecules in B-NPC-1200. We find that the strongly active sites can only be created based on the synergistic effect between nitrogen, boron and oxygen atoms, and the increased density of the active sites are responsible for the lowering of the apparent activation energy in B-NPC-1200 structure. As synthesized B-NPC-1200 exhibits superior catalytic activities for 4-NP reduction with a low apparent activation energy of 27.0 kJ/mol and a high reaction rate constant of $2.3*10^{*-3}$ (s^{-1}). The catalyst can run five times without decreasing significant catalytic activity. The reduction reactions of various nitroarene compounds have been further tested using the B-N PC-1200 material as the precious-metal-free catalyst.

1. Introduction

Carbon-based materials have been demonstrated promising materials for applications including catalysis, energy conversion and storage, nano-electronics, drug delivery, and biomedical applications because of their engineered methodologies and structures by synthetic conditions and exceptional physicochemical properties [1–5]. In particular, three-dimensional (3D) porous carbon-based materials recently have become attractive due to their excellent chemical and mechanical stabilities, controllable porosity, and surface chemistry, superior electrical and thermal conductivities, high specific surface area, good diversity of structure, and potential low synthesis cost [6–8]. Recently, heteroatom doping of carbon-based materials has been reported as an effective method to further alter the band structures, electron transport properties, and surface polarities of carbon-based materials [9–11]. Specifically, co-doping of two different atoms into carbon-based materials could generate a synergistic effect between heteroatom dopants, leading to exceptional improvement of materials' properties as compared to single atom-doped carbon-based materials [12,13]. It has been reported that boron and nitrogen atoms exhibited the most attractive heteroatom-doping pair due to the facile preparation, eco-friendly precursors, and highly efficient activity [14,15]. Consequently, it is important to develop a controllable and scalable synthesis of heteroatom-doped three-dimensional porous carbon-based materials for fundamental studies and applications.

Generally, the 3D structured carbons were synthesized from organic

* Corresponding author at: Department of Chemical Engineering, National Taiwan University, No. 1, Sec. 4, Roosevelt Road, Taipei, 10607, Taiwan.
** Corresponding author.
E-mail addresses: drygchung@gmail.com (Y.G. Chung), whchiang@mail.ntust.edu.tw (W.-H. Chiang), kevinwu@ntu.edu.tw (K.C.-W. Wu).

https://doi.org/10.1016/j.apcatb.2019.117888
Received 28 May 2019; Received in revised form 10 June 2019; Accepted 18 June 2019
Available online 20 June 2019
0926-3373/

molecules or gas molecules as precursors by chemical vapor deposition (CVD) method, leading to hardly morphology control and low surface area [16–19]. Recently, the metal-organic frameworks (MOFs) combined from cationic metals and organic linkers have been shown ideal templates for fabricating various porous carbon-based materials with the higher specific surface area than conventional porous materials and uniform pore size distributions for heterogeneous catalysis [20–23]. It has been demonstrated the excellent catalytic performance in electrochemical properties using MOF-derived 3D porous carbon as a catalyst [24,25]. Moreover, nitrogen-doped porous carbons can be prepared either by *in situ* doping using direct pyrolysis of the nitrogen-containing MOF or post doping through high-temperature annealing of pre-synthesized MOFs with nitrogen-containing precursors [26–29]. Among those MOFs as starting materials for the preparation of heteroatom-doped 3D porous carbons, zeolitic imidazole framework-8 (ZIF-8) has been shown a promising candidate to synthesize nitrogen-doped 3D porous carbon [29–33]. It has been demonstrated that ZIF-8 derived nitrogen-doped porous carbons can be used as an efficient metal-free catalyst for catalysis applications [34–36]. However, the synthesis and fundamental studies of co-doping boron (B) atoms into ZIF-8 derived nitrogen-doped porous carbon (NPC) to construct 3D boron- and nitrogen- co-doped porous carbons (3D-BNPC) are still lacking.

In this article, we synthesized 3D-BNPC with varying nitrogen and boron dopant concentrations using ZIF-8 as a starting material under high-temperature annealing conditions and demonstrated their synergistic effect on catalytic 4-nitrophenol (4-NP) reduction. The overall synthesis steps are shown in Scheme 1, and details are provided in the experimental section. Briefly, 3D-BNPC was synthesized by high-temperature annealing of the mixture of nitrogen-doped porous carbons (NPC) (which was initially prepared from ZIF-8) and boric acid. The synthesized 3D-BNPC samples are denoted as B-NPC-x (x indicates the annealing temperature) in this work. Detailed X-ray photoelectron spectroscopy (XPS) analysis suggests that the B and N atoms can be co-doped into the carbon lattices of the as-synthesized samples. The B concentrations can achieve to 1.5 atomic percentage (at.%) at 1200 °C. Moreover, catalytic-active chemical bindings including quaternary-N (N-Q), BC_2O and BCO_2 were created. The BET specific surface areas of B-NPC-1200 was calculated to be 1299 m^2/g. The four-point probe film-based electrical resistance measurement shows that of the electrical resistance of the B-NPC-1200 was significantly reduced by the factor of 37 times, compared to NPC.

We further performed the catalytic reduction of 4-NP into 4-aminophenol (4-AP) to study the catalytic activity of the as-prepared 3D-BNPC, which is a critical reaction in wastewater treatment and industrial applications [37,38], and expensive noble metals such as Pt, Au, Ag, and Pd, are used as the catalyst [39–44]. The excellent catalytic performance has been observed under the B-NPC-1200 catalyst at room temperature, and B-NPC-1200 catalyst can be recycled and reused for five times without significantly decreasing catalytic activity. Furthermore, the B-NPC-1200 has also demonstrated as useful catalyst for the reduction reaction of nitrobenzene derivatives. Finally, high-resolution X-ray photoelectron spectroscopy (HR-XPS) and density functional theory (DFT) calculations were carried out to confirm the presence of new active sites for 4-NP reduction and to investigate the role of these active sites on 4-NP adsorption energies.

2. Experiment

2.1. Chemicals

Zinc nitrate hexahydrate (98%) and 2-methylimidazole (99%), 4-nitrophenol (4-NP) (99%), 4-aminophenol (4-AP) (99%), 1-chloro-4-nitrobenzene (98%), 1-bromo-4-nitrobenzene (98%), 1-iodo-4-nitrobenzene (98%),4-nitroanisole (98%), 4-nitroaniline (98%) and boric acid (99.5%), were purchased from Sigma-Aldrich or Acros Company and used without further purification.

2.2. Synthesis of 3D nitrogen-doped porous carbon (NPC)

NPC was synthesized by our previous method [35]. In brief, the activated MOF powders (ZIF-8) were carbonized directly under the nitrogen atmosphere at 900 °C for 8 h with a heating rate of 5 °C min^{-1}. After carbonization, the residual zinc component was removed by using concentrated HCl (36.5%). Finally, the resulting samples were washed several times with deionized water and methanol, dried under vacuum condition for the next step.

2.3. Synthesis of 3D B- and N-co-doped porous carbon (3D-BNPC)

The NPC (0.2 g) was added into 20 mL methanol containing boric acid (1 g). The mixture was stirred at RT in 24 h. Then, the methanol was removed by rotary evaporator. The resulted solid was annealed at different temperature (800, 1000, and 1200 °C) for 2 h. After 2 h, the samples were washed by hot water several times for removing unreacted boric acid. The sample name is denoted as B-NPC-x, where x is the annealing temperature.

2.4. Characterizations

Powder X-ray diffraction (XRD) was recorded using a Cu Kα radiation source on a Rigaku-Ultima IV instrument. The morphologies and microstructures of the synthesized samples were observed with scanning electron microscopy (SEM, Nova™ NanoSEM 230) and transision electron microscopy (TEM, JEOL JEM-1200EX II). Element mapping was conducted by high-resolution transision electron microscopy (HRTEM, JEOL-JEM-2100). Nitrogen adsorption/desorption

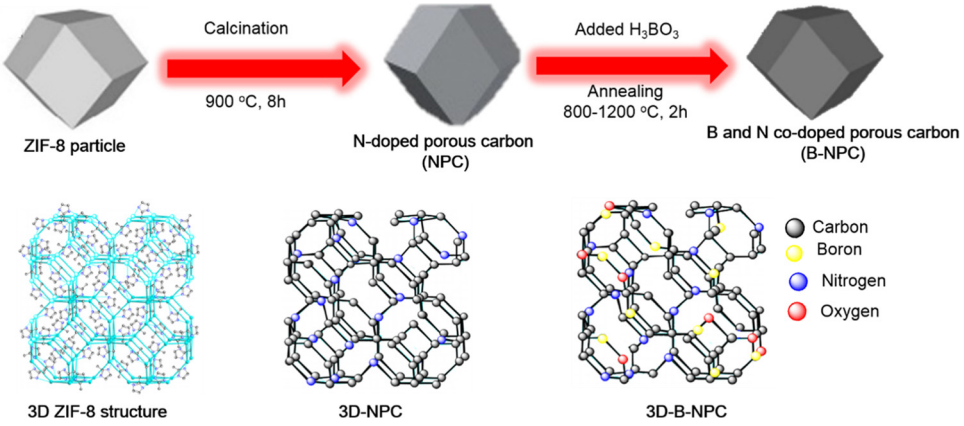

Scheme 1. Synthesis illustration of ZIF-8-derived 3D B and N co-doped porous carbons (3D-BNPCs).

measurements were conducted using a Micromeritics ASAP 2020 for porous properties including specific surface area and pore size. X-ray photoelectron spectroscopy (XPS, Thermo Scientific, Theta Probe), elemental analysis (Elemental Vario EL cube), and Inductively Coupled Plasma-optical emission Spectrometry (ICP-OES) were performed to determine compositions of materials. Raman spectroscopy was performed with a CCD detector at room temperature under excitation of 532 nm. The resistance of synthesized materials was measured using the 4-point probe method (Loresta GP Model MCP-T610, Mitsubishi Chemical). For measurement resistance of the samples, thin films of the materials were prepared the following procedures. Synthesized materials (10 mg) were dispersed in 10 mL isopropanol, the mixture was homogenized at 20000 rpm for 10 min. The resulted mixture was filtered through a polyvinylidene fluoride (PVDF) membrane with the pore size of 1 μm. The solid on the top of the membrane was dried at 60 °C for 24 h. The voltage of instrument was fixed be 10 V for all measurements, the resistances of each sample was averaged from 10 random points

2.5. Catalytic 4-nitrophenol (4-NP) reduction into 4-aminophenol (4-AP) reaction

A 4-NP aqueous solution (0.1 mM) was prepared in advance for all catalyst testing. Typically, a mixture of 4-NP (20 mL, 0.1 mM) and sodium borohydride (5 mL, 0.25 M) as the reducing agent was stirred at RT in 10 min. Then, synthesized catalysts (1 mg) were added into this mixture for the catalytic reduction and stirred (400 rpm) during reaction time. At interval times (2 min), the 1.5 mL reaction solution was withdrawn from reaction solution for reduction analysis using UV–vis absorption spectroscopy (JASCO, V-670).

2.6. Recycle test

To remain and synchronize catalyst during the single reaction of recycling test, the recycle reaction was carried out under optimized reaction condition. Generally, 5 mL solution of sodium borohydride (0.25 M) was added into 4-NP (20 mL, 0.1 mM) and stirred in 10 min. Then, B-NPC-1200 catalyst (2 mg) was added into the mixture. After a reaction time of 20 min, the B-NPC-1200 catalyst was centrifugated and washed by water and methanol several times. The solid catalyst was then dried in vacuum in 12 h before repeating the next reaction.

2.7. Catalytic reduction reaction of nitroarenes

Generally, 2 mL ethanolic solutions containing 0.25 mmol reactants and 3 mg B-N PC-1200 were stirred in 5 min for uniformly mixing. Then, 5 mmol $NaBH_4$ was added into the mixture, following by 2 mL water. The reaction mixture was taken place under magnetic stirring at room temperature. After desire reaction times, the resulting mixture was extracted four times with 20 mL ethylacetate. For calculating reaction conversion, the 5 mL oganic phase was withdrawn and then was mixed with 50 μL n-dodecane as internal standard for gas chromatography (GC) analysis.

2.8. Density functional theory (DFT) calculation

All DFT calculations are carried out using the CP2K Quickstep version 6.1 code which uses the Gaussian Planewave Method (GPW) [45]. The potential energy of a configuration is calculated using the Kohn-Sham density functional theory (KS-DFT) with the spin-polarized implementation of the exchange correlation functional PBEsol [46] along with the D3 dispersion correction of Grimme with Becke-Johnson damping that is parameterized to the PBEsol functional with 10 Å cutoff [47]. The valence electronic densities were computed using MOLOPT-DZVP-SR-GTH basis sets for each atom type [48] and the nuclear and core electronic densities were modelled with spin polarized Goedecker-Teter-Hutter (GTH) pseudopotentials [49,50]. The plane wave is cut off at 1150 Ry with 80 Ry relative cutoff. The plane wave cutoffs were converged with respect to the calculated electronic energies. The electronic energy was minimized with the orbital transformation (OT) method, and the Pulay's direct inversion in the iterative subspace (DIIS) electronic minimizer was used where possible. Conjugate gradients (CG) minimizer was used during energy minimization step optimization step with the following convergence criteria: 1×10^{-4} Å for displacement, and 1×10^{-4} Hartree for the force. The SCF convergence criteria of 1×10^{-6} Hartree were used for the energy minimization and 1×10^{-9} for vibrational analysis. The adsorption energies (E_{ads}) between model surfaces and 4-NP were computed using the Eq. (1):

$$E_{ads} = E_{surface+4NP} - E_{surface} - E_{4NP} \quad (1)$$

where $E_{surface+4NP}$ is the total energy of the system, $E_{surface}$ is the energy of the surface system alone, and E_{4NP} is the energy of 4-NP molecule in the vacuum. Sidik's graphene structure is used as a basis to construct different surface models [51] based on experimental HR-XPS data. Surface models and 4NP ions are independently optimized. Vibrational analyses are carried out for each optimized model to ensure that the system is at the potential energy minimum of the system. The adsorption energies are computed on the optimized surface models and 4-NP molecule where the oxygen atom from 4NP molecule is placed directly on top of different adsorption sites. To locate the minimum, at least 8 single point calculations that are spread evenly between 2.3 Å and 4.0 Å are carried out for each structure. Partial atomic charges of the system were computed using the REPEAT method as implemented in CP2K.

3. Results and discussion

3.1. Characteristics of catalyst

XPS was performed to study the chemical configurations in the as-synthesized samples. From survey XPS spectra (Fig. 1a), we found that the major component in all samples is C (284.6 eV) and followed by minor heteroatoms including N (397.1–402.9 eV), O (530–534 eV) and B (187.5–193.2 eV). The concentration of each element is diverse based on synthesis conditions (**Table S1-2**). The nitrogen concentrations strongly decreased from 11.3 at.% of NPC to 8.5, 4.2, and 1.9 at.% for B-NPC-800, B-NPC-1000, and B-NPC-1200, respectively. On the other hand, there is no boron atom dopant at 800 °C, however, boron atoms can be detected at 1000 °C and 1200 °C, with 0.9 and 1.5 at.%, respectively (**Table S1**). It is confirmed the successful doping of boron into NPC structure, suggesting potential improvement of NPC properties. As shown in **Table S3**, the resistivity of these samples contained boron dopants was significantly reduced by the factor of 10 and 37 times in the presence of 0.9 and 1.5 at.% boron concentration, respectively, compared to others without boron doping. It was reported that the electric conductivity could enhance the electron transfer in electro-catalysis application [36].

Furthermore, the new bonding configurations can be created by boron atoms dopant (Fig. 1b). The B1s and N1s bonding configurations were further studied by high-resolution XPS (HR-XPS). The asymmetric N1s peaks of NPC and B-NPC-x can be deconvoluted into three major bonding configurations including pyridinic-N (N-6) at 398.4 ± 0.2 eV, pyrrolic-N (N-5) at 399.8 ± 0.2 eV, and quaternary-N (N-Q) at 401.1 ± 0.2 eV (Fig. 1**c–f**) [52,53]. In addition, the chemical bonding of boron with carbon atoms in B-NPC-1000 and B-NPC-1200 can be divided as B–C bonds attributing to BC_3 (188.9 ± 0.2 eV), B–N bonds contributing to BNC (190.1 ± 0.2 eV), and C—B—O bonds corresponding to BC_2O (191.2 ± 0.2 eV), and BCO_2 (192.9 ± 0.2 eV) (Fig. 1**g–h**) [54–57]. It may have the B–C–N bonds having an approximate binding energy range of 188–191 eV [54,56], however, which could be overlapped by the BC_3 (188.9 eV), BNC bonds (190.1 eV), and BC2O (191.2 eV). Thus, the exact chemical state of B–C–N bond is not involved in the fitted curves. The diverse configurations of B and N in

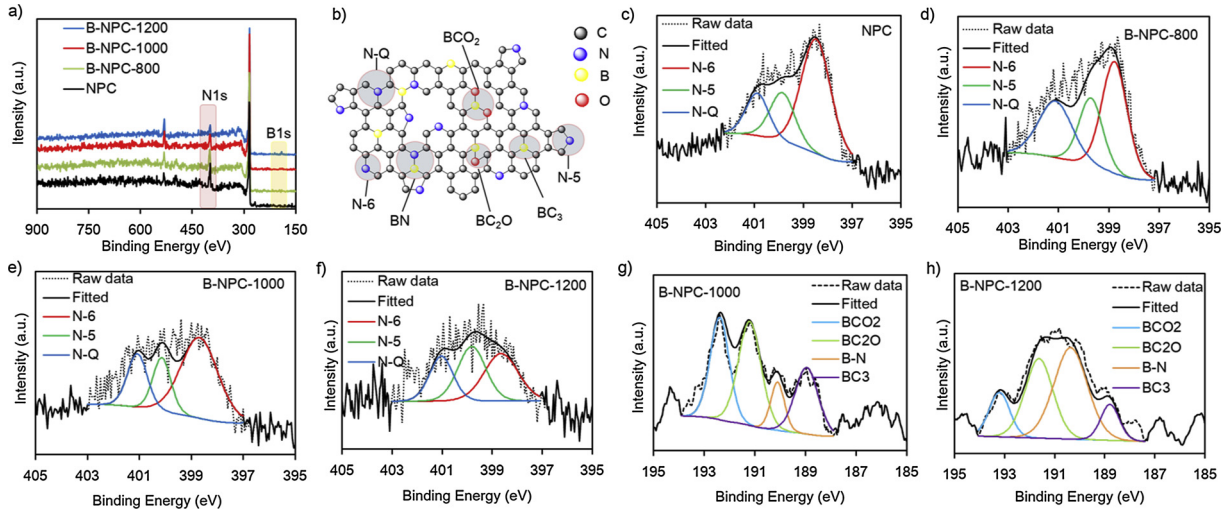

Fig. 1. **a**) Survey XPS spectra of ZIF-8-derived NPC and 3D-BNPCs; **b**) the schematic illustration of various types of B and N atoms configurations in synthesized samples; HRXPS spectra of **c–f**) N1s and **g–h**) B1s.

3D-BNPCs may provide new active sites for catalysis.

The structure of 3D-BNPC was further determined by XRD. The pattern of NPC has two broad peaks at approximately 2θ = 24° and 43°, which belong to (002) and (100) or (101) planes of graphitic carbon, respectively [58,59], indicating that ZIF-8 particles were completely carbonized (Figs. 2**a** and **S1a**). After thermal treatment with boric acid, the (200) and (100) or (101) peak of 3D-BNPC samples are slightly sharper and higher intensity, compared to NPC precursor. We speculate that a certain amount of amorphous carbon has been removed during the boron doping process. In addition, the peak of the plane (002) shifts to lower two-theta degree, corresponding to the increase of boron concentration. This may be due to the changes in the bond length between carbon atoms from addition and removal of heteroatoms, resulting in forming a repulsive force on (002) plane of carbon [1,59].

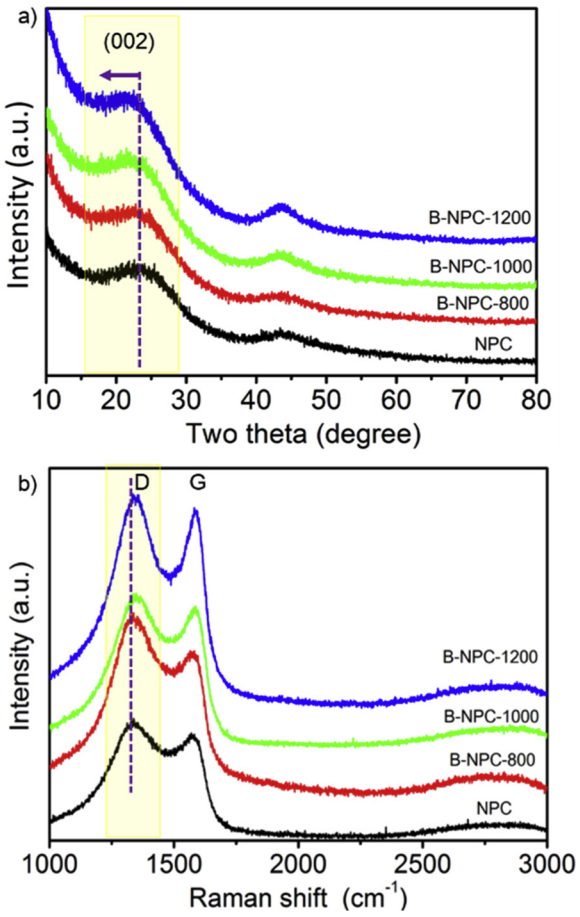

Fig. 2. **a**) XRD patterns and **b**) micro Raman spectra of ZIF-8-derived NPC and 3D-BNPCs.

Raman spectroscopy was additionally carried out to confirm the structural distortion of as-synthesized 3D-BNPC. As shown in Fig. 2b, the as-synthesized samples showed peaks at approximately 1352 cm^{-1} and 1581 cm^{-1} corresponding to D and G band of graphitic carbon, respectively [55]. The D band is due to the defects of the graphitic structure caused by doping of heteroatoms, or empty holes that can induce active sites for catalysis application [1]. On the other hand, G band represents sp2 hybridization carbon of graphene, which is beneficial for electron conductivity [60]. Moreover, we observe that the D bands of B-NPC-1000 and B-NPC-1200 were shifted to higher Raman shift compared to B-NPC-800 and NPC, confirming the result of boron doping. In addition, the I_D/I_G ratios of the synthesized materials are similar, which are 1.10, 1.11, 1.09, and 1.05 for NPC, B-NPC-800, B-NPC-1000, B-NPC-1200, respectively, suggesting the stability of carbon structure.

SEM and TEM were further used to reveal the morphologies of as-synthesized samples. The SEM images indicate the NPC and 3D-BNPC materials still remained similar morphologies as pre-synthesized ZIF-8 (Figs. 3**a–d** and **S1b**) and were with uniform particles size distribution from 100 to 200 nm, suggesting that those samples are highly thermal stable. The SEM-EDX of the synthesized materials indicated the presence of carbon, nitrogen, boron and oxygen (**Fig. S2**), which are in good agreement with XPS and element analysis results. TEM images show that the increasing synthesis temperature led to more clear heterogeneous structure (Fig. 3**e–h**). It is possible that the porosities of these materials were changed due to the doping process. In addition, the HRTEM elemental mapping of B-NPC-1200 exhibits the uniform distributions of carbon, nitrogen, boron and oxygen on the surface of as-prepared sample, suggesting homogeneous distribution of the dopants (**Fig. S3**).

The N_2 adsorption/desorption experiments were carried out to determine specific surface area and pore size distribution. The dosage of absorbed nitrogen gradually increased, corresponding to increased doping temperature (**Fig. S4**). The BET surface areas of NPC, B-NPC-800, B-NPC-1000, and B-NPC-1200 were calculated to be 777, 964, 1157, and 1299 m^2/g, respectively (Table S4). Compared to BN-co-doped graphene in previous reports [16,19,61], our synthesized 3D-

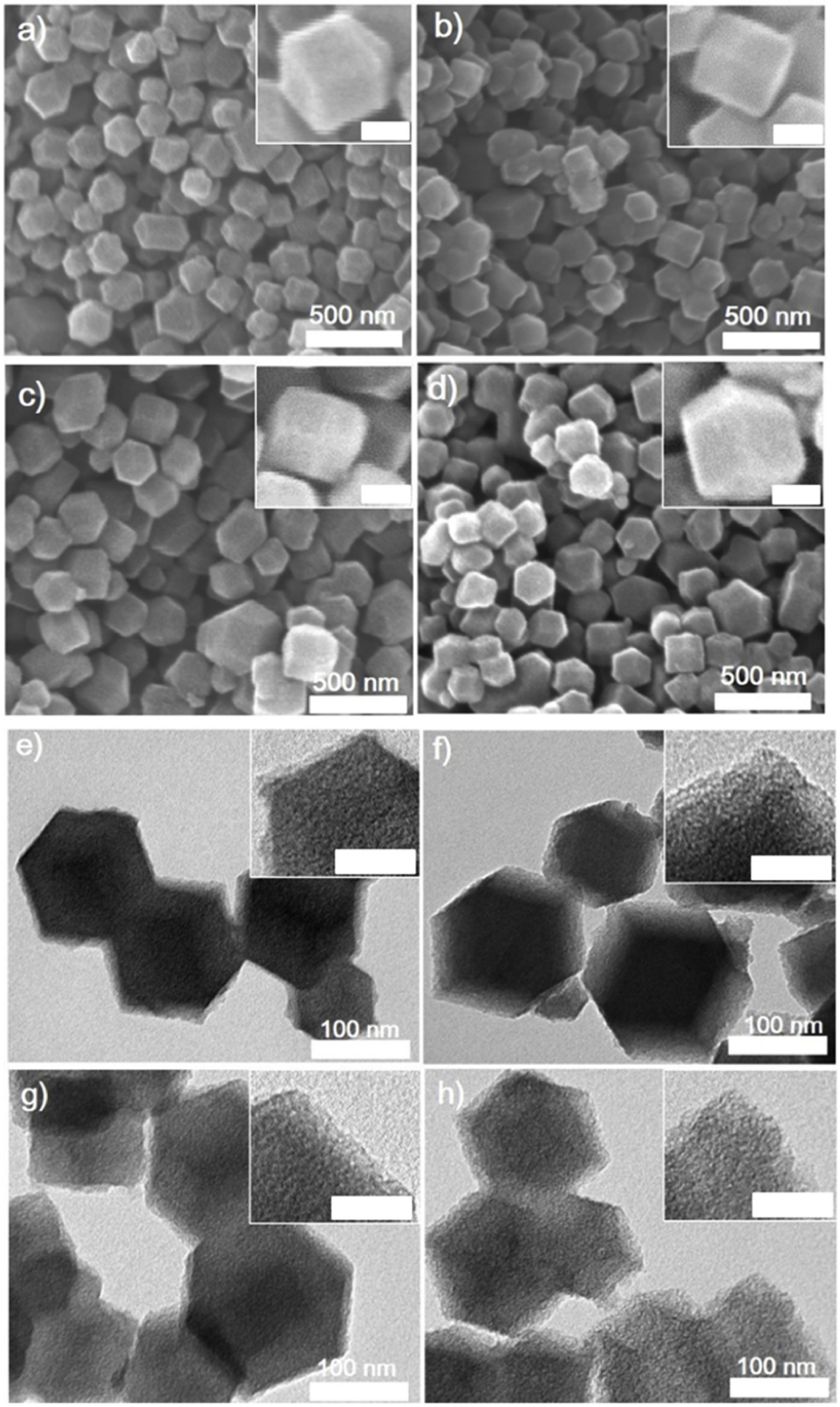

Fig. 3. a–d) SEM and **e–h**) TEM images of NPC, B-NPC-800, B-NPC-1000, and B-NPC-1200 samples, respectively; inside scale bar of 50 nm.

BNPCs show the higher surface area due to 3D structured ZIF-8 precursor. In addition, it is noted that the pore size distribution was shifted to larger pore size, leading to high mesopore volume at high doping temperature (**Fig. S5 and Table S4**). These results are consistent with the TEM analysis (Fig. 2**e–h**). Overall, the high specific surface area and wide pore size distribution are beneficial to the overall increase in the reaction rate and conversion.

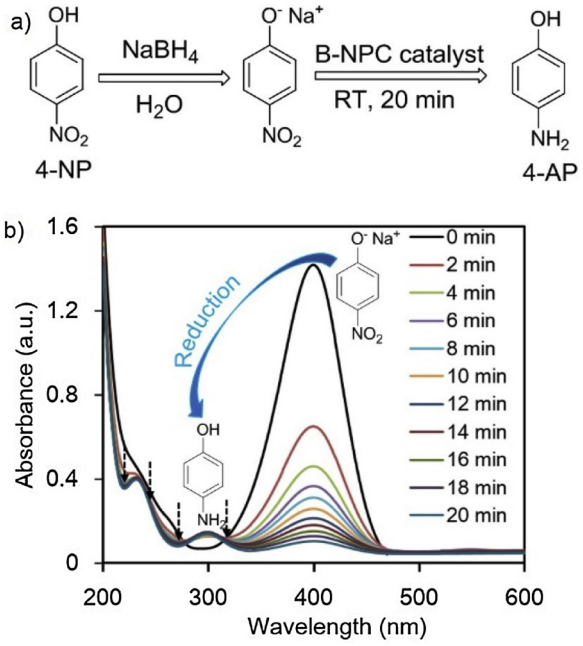

Fig. 4. a) Reaction pathway of 4-NP reduction, **b**) UV–vis spectra of catalytic 4-NP reduction into 4-AP using B-NPC-1200 catalyst (1 mg), reaction condition: 4-NP (20 mL, 0.1 mM), NaBH4 (5 mL, 0.25 M), B-NPC-1200 catalyst (1 mg).

3.2. Catalytic 4-NP reduction into 4-AP studies

The catalytic conversion of 4-NP into 4-AP was introduced to examine the catalytic activity of 3D-BNPC catalyst (Fig. 4a). The quantitative and qualitative progress of 4-NP reduction reaction was observed by UV–vis spectroscopy. In Figs. 4**b** and **S6**, the UV–vis spectra of 4-NP reduction using NPC, B-N PC-800, B-N PC-1000, and B-N PC-1200 catalyst was displayed. The absorption peak of 4-NP ions is at 400 nm, which gradually decreased during reaction time, whereas the increase of peak at 300 nm refers to the 4-AP product. In addition, the four-isosbestic point at 224, 244, 281, and 313 nm indicated that there were no generation of side-products [62,63].

The conversions of 4-NP reductions under various catalysts were shown in Fig. 5**a**. Low conversions of 4-NP were observed to be 16% and 32% at 20 min for NPC and B-NPC-800 catalyst (1 mg), respectively. Significantly, the 4-NP conversion was further increased up to 77% and 94% using B-NPC-1000 and B-NPC-1200 catalyst (1 mg) at 20 min, respectively. It was noticed that NPC and B-NPC-800 catalysts contain no B atoms, while B-NPC-1000 and B-NPC-1200 catalysts contain B on the basis of the XPS analysis (Fig. 1), suggesting that the boron dopants in the 3D-BNPC play a key role for the catalytic performance. The 4-NP ions were further completely converted into 4-AP within 20 and 16 min using 2 and 3 mg of B-NPC-1200 catalyst, respectively (Fig. 5a), indicating that 3D-BNPC catalyst displays an excellent catalytic activity for reduction of 4-NP into 4-AP.

We performed the ICP-OES on all 3D-BNPC catalysts to quantify the residual metal contents in the synthesized materials. NPC and B-NPC-800 show appreciable amount of residual zinc contents (8.2 wt% and 1.9 wt%, respectively) within the structure (**Table S2**). More importantly, we find that the 4-NP is slightly increased for B-NPC-800 material which contains 1.9 wt% of residual zinc atoms. Meanwhile, we find that the 4-NP conversion is significantly increased for B-NPC-1000 and B-NPC-1200 catalysts which contain extremely low amount of residual zinc (0.5 wt% and 0.05 wt%, respectively) (**Table S2**). Furthermore, there were no leaking of Zn during 4-NP reduction that was determined by ICP-OES. On the basis of these results, we conclude that the amount of zinc residues in the catalysts does not affect the 4-NP reduction, and the content of metal play no major role in the catalytic reduction of 4-NP reduction. The possible reason could be that the origin of the zinc in the B-NPC samples were from the zinc oxide structure which generally process a low catalytic activity for 4-NP reduction [64]. In addition, the zinc oxide species may be located inside the pore of B-NPC samples, leading to the poor interaction between 4-NP ions and the zinc oxide species. Another possible reason is because of the usage small amount of B-N PC catalyst (1 mg) in which contained very small amount of zinc (0.5 wt% in B-NPC-100 and 0.05 wt% in B-NPC-1200). Therefore, the effect of Zn on 4-NP conversion can be neglected.

The reaction kinetics of 4-NP reduction using 3D-BNPC catalyst was further investigated. The reaction kinetic data for all catalytic materials tested in this work are tabulated in Table 1. The catalytic conversion of 4-NP into 4-AP has been reported to follow the pseudo-first-order reaction kinetics [39–44], and our results are also consistent with the results from previous investigation, showing a clear linear relationship between reaction time and –ln (1-x), where x is 4-NP conversion (Fig. 5b). The reaction rate constants for B-NPC catalysts from this work and the other reported catalysts are tabulated in **Table S5**. The Arrhenius plots between –ln (k) *vs* 1000/T were constructed to determine the apparent activation energy of the reaction (**Fig. S7**). The apparent activation energies, which is the slope of the Arrhenius plot, of 4-NP under boron-contained B-NPC-1000 and B-NPC-1200 catalysts were 30.2 and 27.0 kJ/mol, respectively. These values are lower than the apparent activation energy calculated for NPC and B-NPC-800 (48.2 and 39.1 kJ/mol, respectively) (**Fig. S7** and Table 1). Because the apparent activation energy of the reaction using B-NPC-1200 catalyst is low as 27.0 kJ/mol, the reaction diffusion limitation needs to be consideration. We further carried out the 4-NP reduction reactions in the absence and presence of magnetic stirring with varying speeds. As showed in **Fig. S8**, there was not significant difference in the 4-NP reaction conversions in the absence and presence of magnetic stirring. A 96% 4-NP conversion was observed under stationary condition while the 4-NP concentrations were completely consumed with stirring speed of 200 rpm and 400 rpm. This result indicates that the diffusion was not key factor for 4-NP reduction in our study.

The reusability of the catalyst was tested to see if the catalyst remains active following the reaction. We find that B-NPC-1200 catalyst can be reused up to 5 times without losing significant activity (Fig. 5c), indicating that B-NPC-1200 catalyst was highly stable during reactions. In addition, the structure of reused B-NPC-1200 catalyst was characterized by XRD, Raman spectroscopy, and N_2 adsorption/desorption. As shown in **Fig. S9a**, the XRD pattern of the fresh B-NPC-1200 catalyst shown similar diffraction peaks to the spent catalyst. The I_D/I_G ratio of the spent B-NPC-1200 catalyst is 1.04, compared to 1.05 for the fresh catalyst (**Fig. S9b**). In addition, the BET surface area of the spent catalyst was calculated to be 1243 m^2/g that is similar to 1299 m^2/g the fresh B-NPC-1200 catalyst (**Fig. S9c**). It can be concluded that the spent B-NPC-1200 catalyst retains similar features to the fresh catalyst, suggesting the stability of B-NPC-1200 catalyst.

We now discuss a few possible contributing factors, such as increased pore sizes and surface areas, and creation of more catalytically active sites for 4-NP reduction, for the increased catalytic activity of 3D-BNPC materials. The increase in the pore size could facilitate the mass transport of reactant molecules to the interior surface of catalyst, and to the active sites for the reaction. However, since the pore sizes are comparable for all catalysts that we investigated in this work, the increased mass transport of reactant molecules alone cannot explain the increased 4-NP conversion between different catalysts. We find that the BET surface area increases from 777 m^2/g to 1299 m^2/g from NPC and B-NPC-1200 structures (**Table S4**). The increased surface area could increase the adsorption rate of 4-NP, which can subsequently lead to higher catalytic conversion of 4-NP molecules to 4-AP. However, the increases in the surface area alone cannot explain the exceptional catalytic activity of B-NPC-1000 and B-NPC-1200. For example, the surface area of 3D-BNPC materials show linear increase with increasing

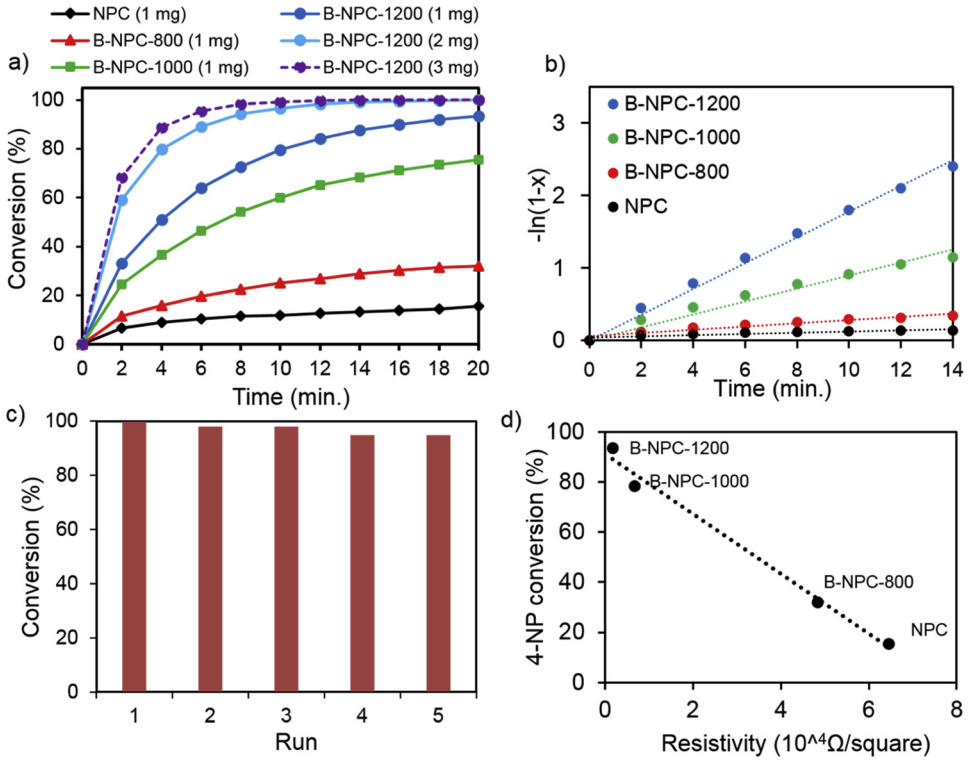

Fig. 5. a) Catalytic performance of synthesized catalysts; reaction condition: 4-NP (20 mL, 0.1 mM) and sodium borohydride (5 mL, 0.25 M), RT, **b**) plots of –ln (1-x) *vs* reaction time, **c**) recycle testing of B-NPC-1200 catalyst, **d**). 4-NP conversion *vs* catalyst resistivity.

Table 1
Reaction rate constants and activated energies of metal-free ZIF-8-derived NPC and 3D-BNPCs catalysts.

Entry	Catalysts	$k*10^{-3}$ (s^{-1})	E (kJ/mol)
1	NPC	0.14	48.2
2	B-NPC-800	0.32	39.1
3	B-NPC-1000	1.80	30.2
4	B-NPC-1200	2.30	27.0

k: reaction rate constant.
E: activation energy.

Table 2
The synergistic effect of co-doping atoms on 4-NP reduction.

Catalysts	4-NP conversion (%)	N/B concentration (at. %)	Activation energy (kJ/mol)
NPC	16	11.3/0	48.2
B-NPC-800	32	8.5/0	39.1
B-NPC-1000	77	4.2/0.9	30.2
B-NPC-1200	94	1.9/1.5	27.0

annealing temperature during the synthesis of these materials. If the increased 4-NP conversion is only due to the increased surface areas, then the 4-NP conversion should increase monotonically with respect to the changes in the surface area of materials. However, this is not the case for B-NPC-1000 and B-NPC-1200, which show 77% and 94% conversion of 4-NP, respectively, compared with 16% and 32% conversion of 4-NP for NPC and B-NPC-800 catalysts (Fig. 5a). Therefore, we suggest that B-NPC-1000 and B-NPC-1200 catalysts may have exceptional active sites that are either not found or inaccessible in NPC and B-NPC-800 structures.

Secondary, the significant increase of electrical conductivity of 3D-BNPC catalysts could accelerate electron transfer on the surface catalyst, providing more proton on active sites of catalyst to enhance 4-NP reduction [65–67]. The evidence is that the 4-NP conversion increases with the decreasing electrical resistivity of 3D-BNPC materials (Fig. 5d). The last factor which contributed an important role to catalytic 4-NP reduction is the catalytic active sites. We find that the 4-NP conversion is significantly increased using B-NPC-1000 and B-NPC-1200 catalysts even though the nitrogen contents of these materials are lower than B-NPC-800 catalyst. However, B-NPC-1000 and B-NPC-1200 catalysts contain 0.9 at.% and 1.5 at.% of boron. On the basis of these results, we propose that the successful heteroatom doping of boron into 3D-BNPC materials creates new active sites that can improve the catalytic conversion of 4-NP into 4-AP. We also found that even though the total concentration of heteroatoms doping (*i.e.* nitrogen and boron dopants) of B-NPC-1000 catalyst is higher than the B-N PC-1200 catalyst, the 4-NP conversion of B-NPC-1000 catalyst is lower than B-NP-1200 catalyst (Table 2). The results suggest that the synergistic effect between nitrogen and boron atoms is necessary to create more catalytic active sties that can increase the catalytic performance as corroborated by the low apparent activation energy and the high reaction rate constants of B-NPC-1000 and B-NPC-1200 compared with NPC and B-NPC-800 materials. Our results are consistent with previous reports from the literature that the synergistic effect can be created by co-doping of nitrogen and boron atoms on carbon materials, resulting in increased catalytic activity [12,13].

3.3. Density functional theory (DFT) calculation

We carried out DFT calculations to illustrate the effect of doped heteroatom on the catalytic reduction of 4-NP. For this purpose, we created several model graphene surfaces based on that mimics the surface of NPC. The optimized model systems and calculated adsorption energy are shown in Figs. 6, **S10** and Table 3. The adsorption energy of 4-NP ions on pristine graphene is –8.7 kJ/mol, which is smaller in magnitude than the values calculated on other heteroatom-doped graphene models (Table 3). This implies the pristine graphene surface does not readily adsorb 4-NP ions as compared to heteroatom doped surface.

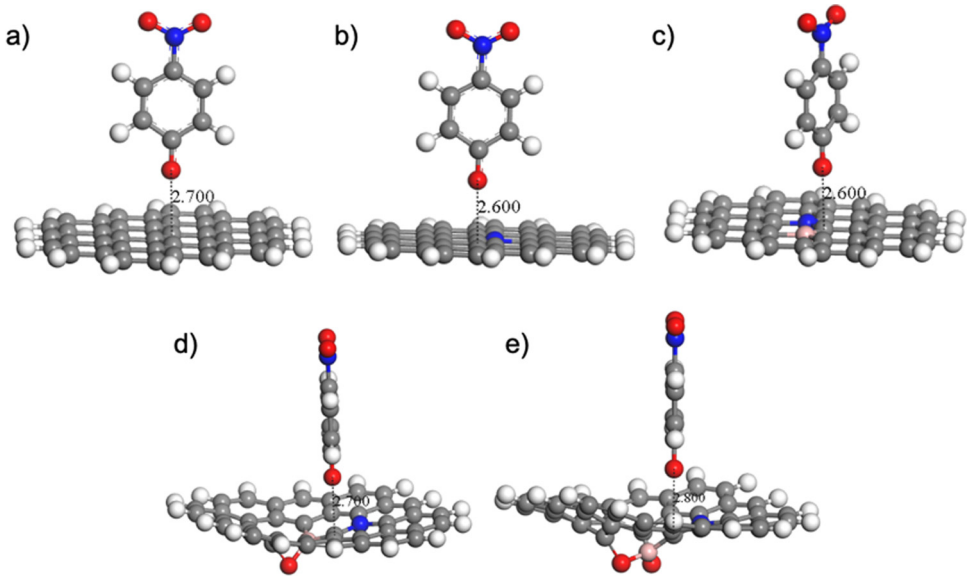

Fig. 6. The optimized structures of 4-NP absorbed on various graphene models, **a**) pristine graphene, **b**) N-Q site of N-co-doped graphene, **c**) N-C-B site, **d**) N-C-BO sites, **e**) N-C-BO2 site of B and N co-doped graphene.

Table 3
Adsorption Energies from DFT Calculations. Smaller the value means the system is more stable.

Model Surfaces	4-NP Adsorption Site	E_{ads} (kJ/mol)	$d_{x\text{-}O}$ (Å)
Pristine graphene	Carbon	−8.70	2.7
N-doped (N-Q)	Carbon	−22.9	2.6
N and B co-doped (N-C-B site)	Carbon	−12.6	2.6
N and B co-doped (N-C-BO site)	Carbon	−20.9	2.7
N and B co-doped (N-C-BO2 site)	Carbon	−29.1	2.8

Different types of catalytic active sites with higher adsorption energies could be created on NPC surface after introducing foreign atoms which is responsible for enhanced catalytic performance [62].

To demonstrate the synergistic effect of boron and nitrogen co-doping on the adsorption energy, we created different active sites models on the basis of XPS data and calculated the adsorption energy of 4-NP ions on these surfaces. According to XPS data, we created three different boron and nitrogen co-doped graphene surfaces with configurations of N-C-B, N-C-BO, and N-C-BO2 (Fig. 6**c–e**). The calculated adsorption energies are –12.6 kJ/mol, –20.9 kJ/mol, and –29.1 kJ/mol, corresponding to N-C-B, N-C2-BO, and N-C-BO2 site, respectively (Table 3). These values are larger in magnitude than the value from the pristine graphene surface, suggesting that the boron and nitrogen co-doped surfaces strongly adsorb 4-NP molecules, which indicate active sites with higher activity. The adsorption energy of 4-NP on N-C-BO2 site is larger in magnitude than the value which was calculated for N-Q site, suggesting that N-C-BO2 site strongly adsorbs the reactant. To further demonstrate the effect of co-doped atoms on the adsorption of 4-NP, we compared the partial atomic charges of optimized structures on boron atoms for N-C-BO and N-C-BO2 structures (**Fig. S11**) before and after the adsorption of 4-NP molecules. We find that the partial atomic charges of the oxygen atom on 4-NP change from –0.403 to –0.174 (N-C-B), –0.082 (N-C2-BO), –0.060 (N-C-BO2), suggesting the possibility of charge transfer between the oxygen atom of 4-NP to doped boron atoms bonded to neighboring oxygen atoms. These computational results demonstrate that the heteroatom doping of boron and nitrogen into porous carbon increases 4-NP reduction, as compared to single nitrogen doping.

3.4. The reduction reaction of various nitroarenes over B-NPC-1200 catalyst

We have further applied the B-NPC-1200 catalyst for the reduction reaction of various nitroarene compounds to demonstrate the catalytic activity of the catalyst. The reduction reactions of the different nitroarenes [68,69] were carried out using $NaBH_4$ as reducing agent in the presence of B-NPC-1200 as the catalyst. As shown in Fig. 7, the B-NPC-1200 catalyst exhibited higher activities for the reduction reaction of 4-nitroaniline and 4-nitroanisole than other nitroarene compounds. This is because that 4-nitroaniline and 4-nitroanisole have an electron-

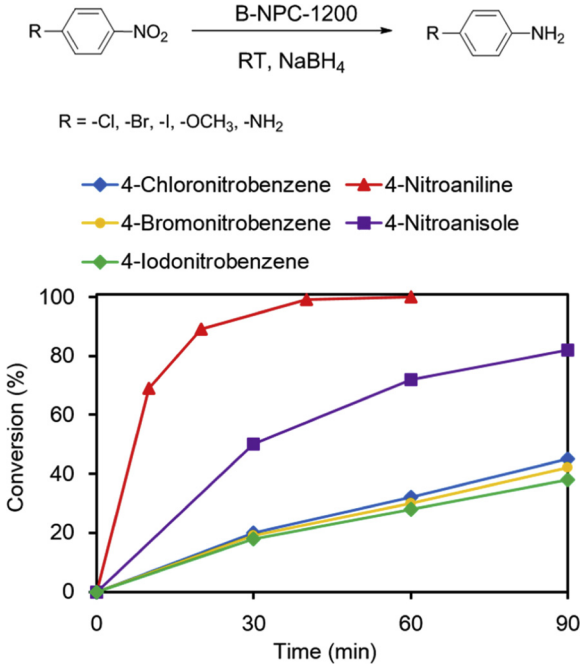

Fig. 7. Reduction reaction of various nitrobenzene compounds over B-N PC-1200 catalyst. Reaction condition: reactants (0.25 mmol), $NaBH_4$ as reducing agent (5 mmol), B-N PC-1200 catalyst (3 mg) H_2O (2 mL), ethanol (2 mL), room temperature. The reaction conversion is determined by GC using n-dodecane as the internal standard.

donating group (such as $–NH_2$ and $–OCH_3$ group, respectively), in contrast of electron-withdrawing groups (such as –Cl, –Br, –I group) in the other nitroarenes. Furthermore, the catalytic activity of B-NPC-1200 catalyst for nitroarenes reduction was compared to other catalyst in the previous reports (**Table S6**). The results clearly indicate that the synthesized B-NPC-1200 material is a promising catalyst for the reduction reaction.

4. Conclusion

We have successfully tailored boron atoms into nitrogen-doped 3D porous carbon materials (NPC) by controlling the annealing temperature. As synthesized 3D-BNPC, particularly the B-NPC-1200 has shown extraordinary properties including high surface area (1299 m^2/g), low resistance (1720 Ω/square), and the strongly catalytic active sites for 4-NP reduction and other nitroarene reductions. The relationships between the surface area, electrical resistance and boron doping with the 4-NP conversion have been demonstrated based on experimental analysis and computational methods. Moreover, the B-NPC-1200 catalyst can be reuse for five times without the loss in the catalytic activity. With dominant physical and chemical properties, the 3D-BNPC catalyst can be applied not only in the catalysis process but also in other applications including sensing, nano-electronics, energy storage and conversion. In addition, it was reported that the morphologies and properties of MOF-derived nanostructured materials (including MOF-derived carbon-based materials) could be controlled *via* rational design and synthesis [20,24]. Therefore, we suggest that the concentrations and types of boron precursor may effect on the structure of MOF-derived heteroatoms-doped carbon such as morphologies and properties. This can inspire to future studies for MOF-derived nanostructured materials.

Declaration of Competing Interest

The authors declare no competing financial interest.

Acknowledgments

We greatly acknowledge the financial support by the Ministry of Science and Technology of Taiwan (Grant no. 104-2628-E-002-008-MY3; 105-2221-E-002-227-MY3; 105-2218-E-155-007; 105-2221-E-002-003-MY3; 105-2622-E155-003-CC2; 107-2628-E-011-002-MY3; 106-2221-E-011-117; 107-2911-I-011-504). Prof. Wu also thank the Aim for Top University Project at National Taiwan University (105R7706; 107L2033-32; 107L891204; 107L7703; 107L104312; 107L7828) and the Center of Atomic Initiative for New Materials, National Taiwan University, from the Featured Areas Research Center Program within the framework of the Higher Education Sprout Project by the Ministry of Education in Taiwan (108L9008) for the funding support. The work used computational resources of the Argonne Leadership Computing Facility, which is a US Department of Energy Office of Science User Facility supported under Contract and not Contract DE-AC02-06CH11357. Y. G. C. acknowledges the support from the Basic Science Research Program through the National Research Foundation of Korea (NRF) funded by the Ministry of Education (NRF-2016R1D1A1B03934484). We also thank the Mass Spectrometry and Transmission Electron Microcopy (JEOL-JEM-2100) Core Facility at Department of Chemistry, National Taiwan University.

Appendix A. Supplementary data

Supplementary material related to this article can be found, in the online version, at doi:https://doi.org/10.1016/j.apcatb.2019.117888.

References

[1] X. Wang, G. Sun, P. Routh, D.-H. Kim, W. Huang, P. Chen, Chem. Soc. Rev. 43 (2014) 7067–7098.
[2] M. Li, F. Xu, H. Li, Y. Wang, Catal. Sci. Technol. 6 (2016) 3670–3693.
[3] M. Pumera, Chem. Soc. Rev. 39 (2010) 4146–4157.
[4] S. Agnoli, M. Favaro, J. Mater. Chem. A 4 (2016) 5002–5025.
[5] J. Liu, L. Cui, D. Losic, Acta Biomater. 9 (2013) 9243–9257.
[6] X.-C. Dong, H. Xu, X.-W. Wang, Y.-X. Huang, M.B. Chan-Park, H. Zhang, L.-H. Wang, W. Huang, P. Chen, ACS Nano 6 (2012) 3206–3213.
[7] Y.-C. Yong, X.-C. Dong, M.B. Chan-Park, H. Song, P. Chen, ACS Nano 6 (2012) 2394–2400.
[8] R.M. Hensleigh, H. Cui, J.S. Oakdale, J.C. Ye, P.G. Campbell, E.B. Duoss, C.M. Spadaccini, X. Zheng, M.A. Worsley, Mater. Horiz. 5 (2018) 1035–1041.
[9] I.-Y. Jeon, S. Zhang, L. Zhang, H.-J. Choi, J.-M. Seo, Z. Xia, L. Dai, J.-B. Baek, Adv. Mater. 25 (2013) 6138–6145.
[10] P. Rani, V.K. Jindal, RSC Adv. 3 (2013) 802–812.
[11] J.-C. Li, P.-X. Hou, C. Liu, Small 13 (2017) 1702002.
[12] S. Wang, E. Iyyamperumal, A. Roy, Y. Xue, D. Yu, L. Dai, Angew. Chem. Int. Ed. 50 (2011) 11756–11760.
[13] Y. Zheng, Y. Jiao, L. Ge, M. Jaroniec, S.Z. Qiao, Angew. Chem. Int. Ed. 52 (2013) 3110–3116.
[14] S. Umrao, T.K. Gupta, S. Kumar, V.K. Singh, M.K. Sultania, J.H. Jung, I.-K. Oh, A. Srivastava, ACS Appl. Mater. Inter. 7 (2015) 19831–19842.
[15] C.H. Choi, M.W. Chung, H.C. Kwon, S.H. Park, S.I. Woo, J. Mater. Chem. A 1 (2013) 3694–3699.
[16] Z.-S. Wu, A. Winter, L. Chen, Y. Sun, A. Turchanin, X. Feng, K. Müllen, Adv. Mater. 24 (2012) 5130–5135.
[17] X. Xie, L. Hu, M. Pasta, G.F. Wells, D. Kong, C.S. Criddle, Y. Cui, Nano Lett. 11 (2011) 291–296.
[18] Z. He, S.D. Minteer, L.T. Angenent, Environ. Sci. Technol. 39 (2005) 5262–5267.
[19] L. Qie, Y. Lin, J.W. Connell, J. Xu, L. Dai, Angew. Chem. Int. Ed. 56 (2017) 6970–6974.
[20] C. Wang, Y.V. Kaneti, Y. Bando, J. Lin, C. Liu, J. Li, Y. Yamauchi, Mater. Horiz. 5 (2018) 394–407.
[21] S.-H. Hsu, C.-T. Li, H.-T. Chien, R.R. Salunkhe, N. Suzuki, Y. Yamauchi, K.-C. Ho, Kevin C.-W. Wu, Sci. Rep. 4 (2014) 6983.
[22] N.L. Torad, Y. Li, S. Ishihara, K. Ariga, Y. Kamachi, H.-Y. Lian, H. Hamoudi, Y. Sakka, W. Chaikittisilp, Kevin C.-W. Wu, Y. Yamauchi, Chem. Lett. 43 (2014) 717–719.
[23] C. Young, J. Wang, J. Kim, Y. Sugahara, J. Henzie, Y. Yamauchi, Chem. Mater. 30 (2018) 3379–3386.
[24] D. Dang, Q.-L. Zhu, Q. Xu, Nat. Rev. Mater. 3 (2018) 17075.
[25] L. Yang, X. Zeng, W. Wang, D. Cao, Adv. Funct. Mater. 28 (2018) 1704537.
[26] H.-X. Zhong, J. Wang, Y.-W. Zhang, W.-L. Xu, W. Xing, D. Xu, Y.-F. Zhang, X.-B. Zhang, Angew. Chem. Int. Ed. 53 (2014) 14235–14239.
[27] N.L. Torad, M. Hu, Y. Kamachi, K. Takai, M. Imura, M. Naito, Y. Yamauchi, Chem. Commun. 49 (2013) 2521–2523.
[28] M.H. Yap, K.L. Fow, G.Z. Chen, Green Energy Environ. 2 (2017) 218–245.
[29] R.R. Salunkhe, C. Young, J. Tang, T. Takei, Y. Ide, N. Kobayashi, Y. Yamauchi, Chem. Commun. 52 (2016) 4764–4767.
[30] W. Zhang, X. Jiang, Y. Zhao, A.C.S. anchez, V. Malgras, J. Kim, J.H. Kim, S. Wang, J. Liu, J.-S. Jiang, Y. Yamauchi, M. Hu, Chem. Sci. 8 (2017) 3538–3546.
[31] S. Gadipelli, Z.X. Guo, ChemSusChem 8 (2015) 2123–2132.
[32] J. He, R.C.C. Yap, S.Y. Wong, Y. Zhang, Y. Hu, C. Chen, X. Zhang, J. Wang, X. Li, CrystEngComm 18 (2016) 5262–5266.
[33] Y. Yusran, D. Xu, Q. Fang, D. Zhang, S. Qiu, Microporous Mesoporous Mater. 241 (2017) 346–354.
[34] Y. Wang, L. Tao, Z. Xiao, R. Chen, Z. Jiang, S. Wang, Adv. Funct. Mater. 28 (2018) 1705356.
[35] C.V. Nguyen, Y.-T. Liao, T.-C. Kang, J.E. Chen, T. Yoshikawa, Y. Nakasaka, T. Masuda, Kevin C.-W. Wu, Green Chem. 18 (2016) 5957–5961.
[36] J. Wei, Y. Hu, Y. Liang, B. Kong, J. Zhang, J. Song, Q. Bao, G.P. Simon, S.P. Jiang, H. Wang, Adv. Funct. Mater. 25 (2015) 5768–5777.
[37] N. Sahiner, S. Yildiz, H. Al-Lohedan, Appl. Catal. B: Environ. 166–167 (2015) 145–154.
[38] J. Xia, G. He, L. Zhang, X. Sun, X. Wang, Appl. Catal. B: Environ. 180 (2016) 408–415.
[39] L.-M. Lyu, Y.-C. Kao, D.A. Cullen, B.T. Sneed, Y.-C. Chuang, C.-H. Kuo, Chem. Mater. 29 (2017) 5681–5692.
[40] Y.-T. Liao, J.E. Chen, Y. Isida, T. Yonezawa, W.-C. Chang, S.M. Alshehri, Y. Yamauchi, K.C.-W. Wu, ChemCatChem 8 (2016) 502–509.
[41] X. Song, H. Sun, X. Cao, Z. Wang, D. Zhao, J. Sun, H. Zhang, X. Li, RSC Adv. 6 (2016) 112451–112454.
[42] H.-L. Jiang, T. Akita, T. Ishida, M. Haruta, Q. Xu, J. Am. Chem. Soc. 133 (2011) 1304–1306.
[43] N. Muthuchamy, A. Gopalan, K.-P. Lee, RSC Adv. 5 (2015) 76170–76181.
[44] C. Wang, H. Zhang, C. Feng, S. Gao, N. Shang, Z. Wang, Catal. Comm. 72 (2015) 29–32.
[45] J. Hutter, M. Iannuzzi, F. Schiffmann, J. VandeVondele, WIREs Comput. Mol. Sci. 4 (2014) 15–25.
[46] G.I. Csonka, J.P. Perdew, A. Ruzsinszky, P.H.T. Philipsen, S. Lebègue, J. Paier, O.A. Vydrov, J.G. Ángyán, Phys. Rev. B 79 (2009) 155107.
[47] S. Grimme, J. Antony, S. Ehrlich, H. Krieg, J. Chem. Phys. 132 (2010) 154104.
[48] J. Vande Vondele, J. Hutter, J. Chem. Phys. 127 (2007) 114105.

[49] S. Goedecker, M. Teter, J. Hutter, Phys. Rev. B 54 (1996) 1703–1710.
[50] C. Hartwigsen, S. Goedecker, J. Hutter, Phys. Rev. B 58 (1998) 3641–3662.
[51] R.A. Sidik, A.B. Anderson, J. Phys. Chem. B 110 (2006) 1787–1793.
[52] F. Zheng, Y. Yang, Q. Chen, Nat. Commun. 5 (2014) 5261.
[53] Y. Tong, P. Chen, T. Zhou, K. Xu, W. Chu, C. Wu, Y. Xie, Angew. Chem. Int. Ed. 56 (2017) 7121–7125.
[54] S. Baik, J.W. Lee, RSC Adv. 5 (2015) 24661–24669.
[55] W.-H. Chiang, G.-L. Chen, C.-Y. Hsieh, S.-C. Lo, RSC Adv. 5 (2015) 97579–97588.
[56] A. Perrone, A.P. Caricato, A. Luches, M. Dinescu, C. Ghica, V. Sandu, A. Andrei, Appl. Surf. Sci. 133 (1998) 3239–3242.
[57] M.A. Mannan, M. Nagano, K. Shigezumi, T. Kida, N. Hirao, Y. Baba, Am. J. Appl. Sci. 5 (2007) 736–741.
[58] G. Srinivas, Y. Zhu, R. Piner, N. Skipper, M. Ellerby, R. Ruoff, Carbon 48 (2010) 630–635.
[59] F.M. Hassan, V. Chabot, J. Li, B.K. Kim, L. Ricardez-Sandoval, A. Yu, J. Mater. Chem. A 1 (2013) 2904–2912.
[60] K.N. Kudin, B. Ozbas, H.C. Schniepp, R.K. Prud'homme, I.A. Aksay, R. Car, Nano Lett. 8 (2008) 36–41.
[61] Z. Chen, W. Ren, L. Gao, B. Liu, S. Pei, H.-M. Cheng, Nat. Mater. 10 (2011) 424–428.
[62] X.-K. Kong, Z.-Y. Sun, M. Chen, C.-L. Chen, Q.-W. Chen, Energy Environ. Sci. 6 (2013) 3260–3266.
[63] Y. Mei, Y. Lu, F. Polzer, M. Ballauff, Chem. Mater. 19 (2007) 1062–1069.
[64] B. Divband, M. Khatamian, G.R.K. Eslamian, M. Darbandi, Appl. Surf. Sci. 284 (2013) 80–86.
[65] P. Adelroth, H. Sigurdson, S. Hallen, P. Brzezinski, Proc. Natl. Acad. Sci. U. S. A. 93 (1996) 12292–12297.
[66] A. Nitzan, J. Phys. Chem. A 105 (2001) 2677–2679.
[67] E. Antolini, Appl. Catal. B: Environ. 88 (2009) 1–24.
[68] S. Cai, H. Duan, H. Rong, D. Wang, L. Li, W. He, Y. Li, ACS Catal. 3 (2013) 608–612.
[69] M. Hosseini-Sarvari, Z. Razmi, Appl. Surf. Sci. 324 (2015) 265–274.